NANOPHOTONICS

Spatiotemporal imaging of 2D polariton wave packet dynamics using free electrons

Yaniv Kurman[1]†, Raphael Dahan[1]†, Hanan Herzig Sheinfux[2], Kangpeng Wang[1], Michael Yannai[1], Yuval Adiv[1], Ori Reinhardt[1], Luiz H. G. Tizei[3], Steffi Y. Woo[3], Jiahan Li[4], James H. Edgar[4], Mathieu Kociak[3], Frank H. L. Koppens[2,5]*, Ido Kaminer[1]*

Coherent optical excitations in two-dimensional (2D) materials, 2D polaritons, can generate a plethora of optical phenomena that arise from the extraordinary dispersion relations that do not exist in regular materials. Probing of the dynamical phenomena of 2D polaritons requires simultaneous spatial and temporal imaging capabilities and could reveal unknown coherent optical phenomena in 2D materials. Here, we present a spatiotemporal measurement of 2D wave packet dynamics, from its formation to its decay, using an ultrafast transmission electron microscope driven by femtosecond midinfrared pulses. The ability to coherently excite phonon-polariton wave packets and probe their evolution in a nondestructive manner reveals intriguing dispersion-dependent dynamics that includes splitting of multibranch wave packets and, unexpectedly, wave packet deceleration and acceleration. Having access to the full spatiotemporal dynamics of 2D wave packets can be used to illuminate puzzles in topological polaritons and discover exotic nonlinear optical phenomena in 2D materials.

Understanding of the propagating optical polaritons in two-dimensional (2D) materials has progressed from a promising concept (*1*) to a platform for demonstrating rich physical phenomena (*2*) and is now having an impact on emerging opto-electronics (*3*) and nanophotonic technologies (*4*, *5*). These polaritons exhibit relatively low loss and long propagation distances, simultaneous with extreme confinement factors (*6*–*8*), which facilitates their light-matter interactions (*9*–*11*).

There is motivation to use the distinctive properties of 2D polaritons and integrate them into ultrafast optical technologies that rely on the spatiotemporal control of light. Conventional areas of ultrafast optics achieve such control using pulse-shaping (*12*) and dispersion engineering, which are instrumental, for example, in photonic waveguides (*13*). The attainment of similar control with 2D polaritons could promote the integration of 2D polaritonic materials in mature areas of science and technology and contribute to their fundamental understanding. However, the spatiotemporal control of 2D polariton wave packets has remained out of reach for exactly the same reasons that make their potential applications exciting: They have extremely small wavelengths and are strongly confined inside the material. New capabilities are necessary for accessing the spatiotemporal dynamics of 2D polaritons and their wave packets with nanometric spatial resolution and femtosecond temporal resolution.

In this regard, it is particularly interesting to consider wave packets in materials that exhibit hyperbolic dispersion (*14*, *15*): Polaritons in hyperbolic materials show rich physical behavior, ranging from negative refraction (*16*) and subdiffraction imaging (*14*) to effective Hawking radiation. Although hyperbolic dispersion was originally observed in metamaterials, phonon-polariton (PhP) excitations in 2D materials also exhibit hyperbolic dispersion (*8*, *17*); the phononic resonance creates a dispersion relation that contains multiple branches (see Fig. 1B), which were shown to be tunable by the 2D material geometry, thickness, and surrounding environment (*4*, *5*, *17*), reaching high confinement with relatively low losses, even at room temperature (*6*).

The peculiar dynamics of hyperbolic wave packets can be seen by looking at the group velocity: The derivative of the dispersion, $\partial\omega/\partial k$ (where ω is the radial frequency and k is the wave number), approaches zero in a hyperbolic medium, because the medium supports excitations with (in principle) arbitrarily large momenta. In practicality, the group velocity of PhPs is well defined, given an excitation of a finite bandwidth exciting a specific branch. However, in 2D hyperbolic materials, any coherent excitation is expected to simultaneously stimulate multiple PhP branches, each having different dynamics. Moreover, even a small variation in the excitation's bandwidth or frequency results in a large change in the polariton group velocity and the entire wave packet propagation dynamics. These prospects are especially intriguing in 2D hyperbolic materials such as thin flakes of hexagonal boron nitride (hBN), where the group velocity of polaritons was shown be as low as $c/500$ (with c being the speed of light in vacuum) over a relatively wide bandwidth (*18*). To explore these prospects of hyperbolic wave packets and reveal their physics, we need access to the field comprising the wave packet during its evolution inside the 2D material.

Coherent wave packet dynamics

Our approach to measuring the spatiotemporal dynamics of hyperbolic PhP wave packets inside isotopically pure hBN (^{11}B) flakes (*6*) is made possible by exploiting the interaction between free electrons and PhP wave packets. The temporal dynamics is obtained using a pump-probe technique with a mid–infrared (IR) laser pump and a free-electron probe in an ultrafast transmission electron microscope (UTEM) (*19*–*28*) (Fig. 1A). The pulsed free electron penetrates the sample and consequently changes its energy spectrum according to the integrated electric field along its path (insets of Fig. 1C). Through energy filtering of the postinteraction electron, we can reconstruct the image of the PhP wave packet. The use of laser-driven energy-filtered transmission electron microscopy (EFTEM) was first demonstrated in photon-induced near-field electron microscopy (PINEM). Our approach takes PINEM to the mid-IR range and combines it with 2D materials, providing a test of dispersion models of 2D materials in the time domain.

We recorded the PhP wave packet creation and propagation [Fig. 1D and movies S1 and S2 (*29*)], revealing rare physical behaviors, such as multibranch wave packet splitting, acceleration, and deceleration. The measured acceleration and deceleration dynamics are especially surprising because wave packets conventionally have a fixed group velocity. In certain cases, as in the thin hyperbolic hBN flakes, the group velocity is expected to be very slow—indeed, we observed group velocities from $c/45$ to $c/850$—and still, each wave packet is expected to propagate with a fixed group velocity. In contrast to this expectation, we show that the dispersive nature of PhPs (i.e., their momenta change rapidly in frequency) facilitates acceleration and deceleration dynamics. This result serves as a key example for the rich physical phenomena that can be found when probing the spatiotemporal dynamics of 2D polaritons in a nondestructive manner when combining the femtosecond temporal and nanometer spatial resolution of the UTEM.

Imaging 2D polariton excitations

Among the various experimental techniques used in the field of 2D polaritons, scanning nearfield optical microscopy (SNOM) and its variants have had the most impact so far on the direct near-field imaging of 2D polaritons (*6*, *17*, *30*). Recent advances in time-resolved

[1]Department of Electrical and Computer Engineering, Technion–Israel Institute of Technology, 32000 Haifa, Israel. [2]ICFO-Institut de Ciències Fotòniques, The Barcelona Institute of Science and Technology, Av. Carl Friedrich Gauss 3, 08860 Castelldefels (Barcelona), Spain. [3]Laboratoire de Physique des Solides, Université Paris-Saclay, CNRS, 91405 Orsay, France. [4]Tim Taylor Department of Chemical Engineering, Kansas State University, Manhattan, KS 66506, USA. [5]ICREA-Institució Catalana de Recerca i Estudis Avanats, Passeig Lluís Companys 23, 08010 Barcelona, Spain.
*Corresponding author. Email: kaminer@technion.ac.il (I.K.); frank.koppens@icfo.eu (F.H.L.K.)
†These authors contributed equally to this work.

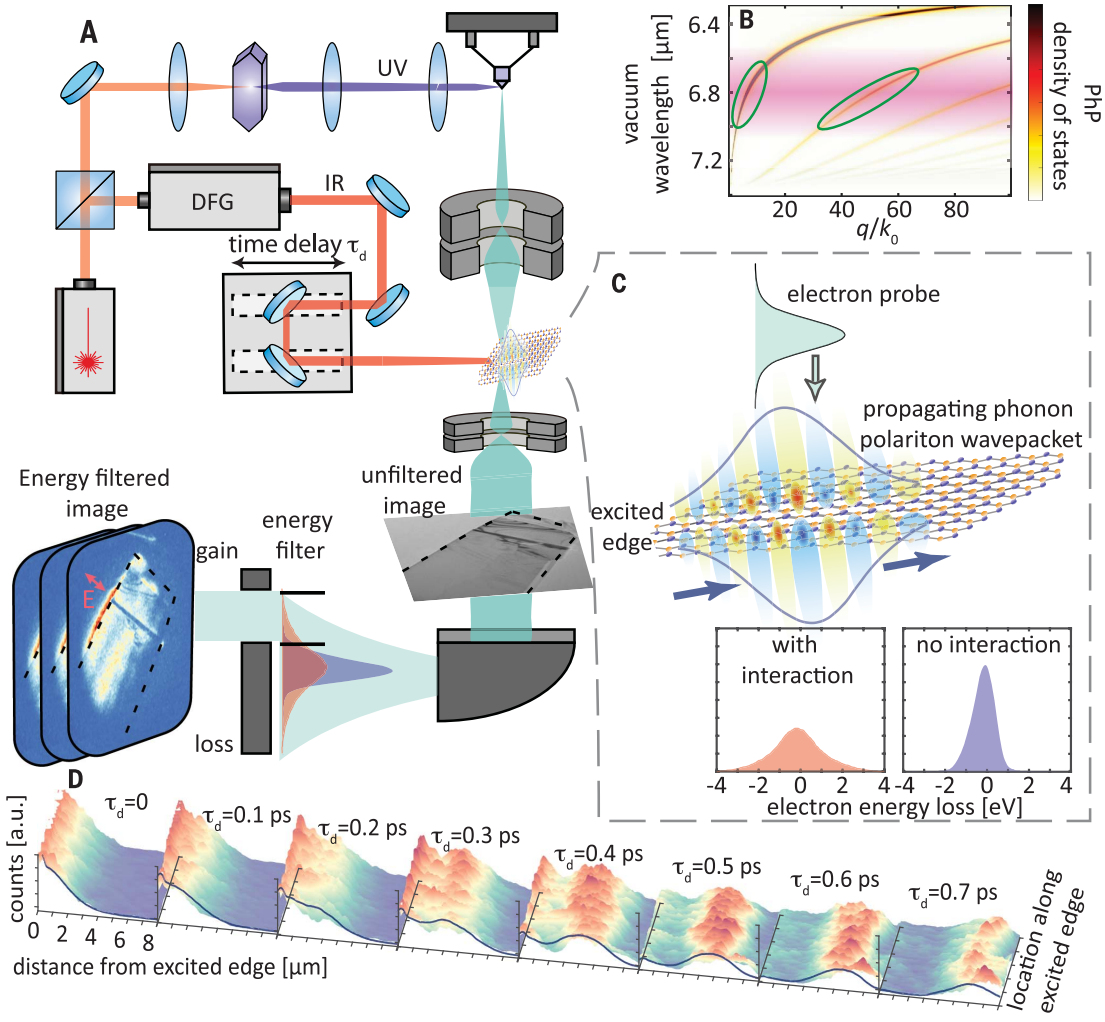

Fig. 1. Direct observation of 2D polariton wave packets using UTEM. (**A**) Experimental setup. A femtosecond laser (orange) splits into two branches. The bottom branch is converted into a mid-IR (red) pulse using difference frequency generation (DFG) and excites the PhP wave packet in the isotopically pure hBN (^{11}B) sample. The top branch is converted into an ultraviolet (UV; purple) pulse using fourth-harmonic generation and photoelectrically excites the electron pulse (cyan). The electron images the hBN sample when counting electrons at all energies (unfiltered image) and images the PhP wave packet when counting only electrons that gained energy (filtered image). E, the IR-pulse electric field. (**B**) Dispersion relation of a 55-nm-thick isotopically pure hBN (^{11}B) flake on a 20-nm-thick Si_3N_4 membrane [for sample preparation, see (*29*)]. The hyperbolic nature of hBN creates multiple dispersion branches in each frequency, each creating a different propagating wave packet. The spectral bandwidth of the IR pulse (pink) excites a range of polariton modes (circled in green). q/k_0, the PhP-photon wave number ratio. (**C**) Free electron probing the (TM polarized) propagating PhP wave packet inside the hBN. The insets show EELS spectra with the laser on (left) and off (right). (**D**) Measurement of the energy-filtered electrons for different time delays τ_d between the laser pulse and the electron probe, showing the propagation dynamics of the PhP wave packet (shown in the top view in fig. S1 and in movie S1). Note that the definition of τ_d is up to arbitrary shifts in all figures and movies. a.u., arbitrary units.

SNOM also allowed the polariton's properties as group velocity to be extracted from the interference of scattered polaritons with different time delays (*18*, *31*–*33*). However, this interferometric technique cannot image the wave packet dynamics, because it does not include the spectral phase, i.e., the phase difference between photons of different wavelengths. Other important experimental approaches, such as photoemission electron microscopy (*34*), are also used for near-field imaging in plasmonics; these approaches, thus far, have not accessed the mid- and far-IR regions. We discuss the different experimental approaches in the supplementary text (*29*). Importantly, techniques based on TEM stand out from all of the above because the electron penetrates through the sample and also becomes sensitive to the buried field rather than only to the field on the surface (*23*), an advantage for probing the highly confined 2D polaritons.

Our approach for the observation of PhP wave packet dynamics adds to the toolbox of electron-beam spectroscopy and microscopy (*35*). Of particular importance for our approach are the advances in the imaging of polaritons using electron energy-loss spectroscopy (EELS) (*36*), which is able to measure IR excitations in vibrational electron spectroscopy (*37*). EELS enabled the measurement of purely vibrational modes (phonons) in bulk media and on surfaces (*38*) and the extraction of their dispersion relations using electron imaging and diffraction (*39*). In recent years, the improvements in the energy resolution of EELS (*37*) enabled the extraction of the PhP dispersion in extremely thin samples (*40*). Such experiments translated methodologies in electron microscopy, once applied to plasmons in the visible range [e.g., (*41*)], to phonons in the mid-IR range.

In all these EELS experiments, one obtains static, time-independent information on the polaritonic modes and other excitations of the sample, all of which are triggered by the free electron. By contrast, PINEM-based techniques such as ours use the electron only as a time-dependent probe (and not as a trigger of the excitation); thus, PINEM allows the extraction of time-dependent information on the temporal dynamics of the polaritons that are excited by a separate laser pulse.

Wave packet creation and propagation

Figure 1D and movie S1 present an example of the measurements made of the wave packet during its creation and propagation inside the flake. The video is created by repeating the measurement for a range of time delays between the laser pump and the electron probe. Such measurements of wave packet dynamics rely on stimulated free electron–PhP interactions. For the wave packet, the electron is a nondestructive probe: The interaction alters the wave packet

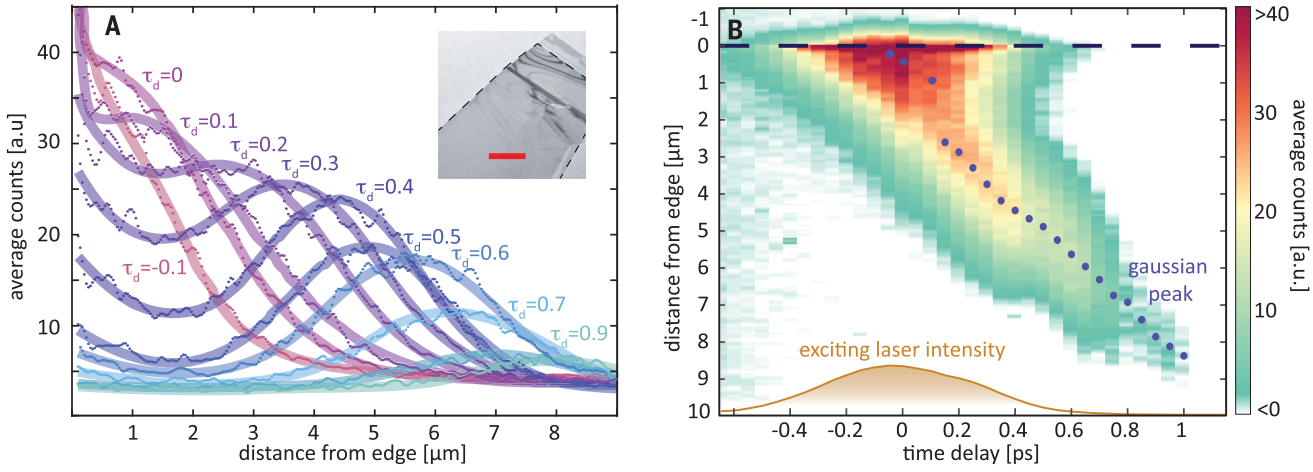

Fig. 2. Direct observation of the PhP wave packet's spatiotemporal dynamics. (**A**) Measured signal when averaged along the edge direction (dots) with the fit of a Gaussian profile plus an exponential decay for each measurement. The times are reported in picoseconds. The inset shows an unfiltered image of the hBN flake; the scale bar is 5 μm. (**B**) Map presenting the measured wave packet as a function of time and distance from the edge; the blue dots represent the Gaussian wave packet peak, and gold represents the laser excitation intensity. At short times, while the laser is still on, the group velocity undergoes changes. Here, the time delay τ_d = 0 is related to the peak of the excitation intensity. This measurement uses a 55-nm-thick hBN flake, excited by a 6470-nm laser with a bandwidth of 175 nm.

in a negligible manner and hence does not interfere with the wave packet evolution dynamics. Thus, the wave packet propagates across the sample uninterrupted, starting from a single edge [chosen by optimizing the laser coupling (*29*)]. At each time delay, the wave packet profile is reconstructed from the electron energy distribution: At points where the PhP's out-of-plane electric field is stronger, there is a larger probability for the probing electron to gain energy and pass an energy filter. The energy filter is chosen to maximize the signal (see fig. S4); it creates a threshold for the detectable PhP field and thus reduces the signal-to-noise ratio. Consequently, as we describe in the theory below, the connection between the number of counts and the electric field is nonlinear.

To model the free electron–PhP interaction, we find it essential to generalize the single-frequency theory of conventional PINEM (*20*, *21*) that was used to describe most PINEM experiments to date. The need to go beyond the successful PINEM theory lies in the finite bandwidth of the excitation laser (necessary for creating the pulsed PhP wave packet) that excites the highly dispersive hBN PhPs. To capture the spectral bandwidth, we describe the free electron–PhP coupling through a generalized coupling function $g(x, y, \omega)$. This coupling function g quantifies the strength of the interaction for each in-plane coordinate (x, y) and each frequency ω. According to this continuous-PINEM theory (*42*)

$$g(x,y,\omega)=\frac{e}{\hbar\omega}\int_{-\infty}^{\infty}dz E_z(x,y,z,\omega)e^{-i\frac{\omega}{v}z} \quad (1)$$

where e and v are the electron charge and velocity, respectively, and $\hbar$ is the reduced Planck's constant. The integral is performed along the electron propagation direction z, on the z component of the electric field phasor $E_z(\omega)=\int E_z(t)e^{i\omega t}dt$, which includes all the PhP modes due to their transverse magnetic (TM) polarization.

The PhP wave packet is imprinted on the electron as a time-dependent phase modulation:

$$\exp\left(2i\int_0^{\infty}d\omega|g(x,y,\omega)|\sin\{\omega t-\arg[g(x,y,\omega)]\}\right) \quad (2)$$

This phase modulation multiplies the initial electron wave function with a time delay (τ_d) relative to the PhP wave packet excitation; τ_d is shifted for recording a video of the dynamics. Our theory predicts the measured electron energy spectra as the Fourier transform (time→ energy) of the resulting electron wave function. Equation 2 shows how larger g values imply stronger modulation in the phase of the free-electron wave function, equivalent to the electron gaining and losing more energy (*29*). The energy required for a detectable signal is related to the incoherent energy width of the preinteraction electron (also called zero-loss peak). Because the width (0.9 eV in our system; right inset of Fig. 1C) is larger than the energy of a single PhP quanta, the postinteraction EELS spectrum (left inset of Fig. 1C) does not have discrete peaks as in PINEM experiments in the visible or near-IR range (*26*). Nevertheless, the change in the electron's energy is sufficient for probing the PhP wave packet: The electron image in the x-y plane is filtered by energy for different time delays τ_d to extract the PhP spatiotemporal dynamics.

In the analysis of the measured PhP wave packet dynamics, we first extract the field profile along the direction of propagation (Fig. 2A). When averaging the signal along the sample's excited edge, we reduce the signal-to-noise ratio [described in (*29*)]. We find that a combination of a Gaussian and an exponential decay due to the edge effect provide a good fit to the measured wave packet, which can also capture the slowly moving higher branches quite accurately. This analysis reveals the formation of the wave packet during the arrival of the excitation pulse. Figure 2B shows an intriguing phenomenon: The wave packet appears to remain stuck at the edge for a certain time duration and does not immediately propagate away from the boundary. Instead, the wave packet's width and amplitude gradually increase. Thus, the gradually forming wave packet increases in amplitude while remaining near the edge. Only toward the end of the excitation pulse (when its tail arrives) does the wave packet start to move away from the edge more quickly, exhibiting phenomena of acceleration and deceleration that vary between samples and excitation wavelengths. Once the excitation pulse has ended, we can extract the stable group velocities.

The wave packet properties during its formation, propagation, and gradual decay are summarized for three different samples and a range of excitation pulses (Fig. 3, A to C). As expected, the group velocities become smaller as the sample thickness decreases. The lowest measured group velocity (light blue in Fig. 3A) is 0.35 μm/ps, which is 860 times

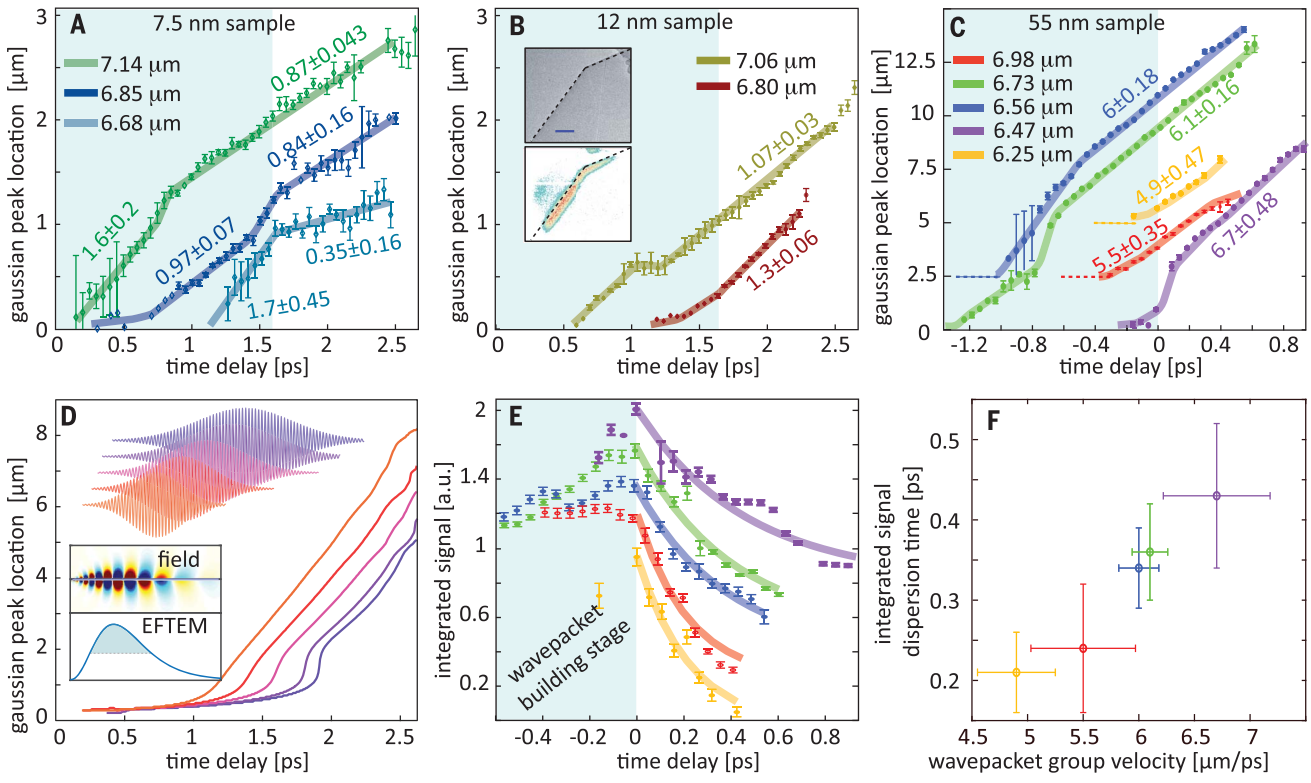

Fig. 3. Analysis of the PhP wave packet formation, propagation, and decay—extracting the group velocities and wave packet behavior. (**A** to **C**) The fitted Gaussian peak locations as a function of time with the extracted group velocities in units of μm/ps. We compare three h^{11}BN samples that have thicknesses of (A) 7.5 nm, (B) 12 nm, and (C) 55 nm. For a better visualization, each measurement is shifted in time to a fixed end time of the pumping (shaded background) and shifted in space (by 0, 2.5, or 5 μm) as marked by dashed horizontal lines in (C). See table S1 for excitation profiles. The top inset in (B) shows an unfiltered image of the 12-nm sample (dashed lines represent sample edges); scale bar is 5 μm. The bottom inset in (B) shows an electron energy loss–filtered image showing the group at a specific time. (**D**) Simulation results of the wave packet peak location as a function of time in a 55-nm h^{11}BN sample on a 20-nm Si_3N_4 membrane, comparing different levels of chirp. (The excitations' temporal profiles are brought above the curves.) The simulations show the acceleration and deceleration that are observed experimentally. The top inset shows the simulated field. The bottom inset shows the energy-filtered electron signal calculated using the field from the top inset, showing that the PINEM technique indeed extracts the wave packet profile. Further simulations of the velocity change can be seen in fig. S5 and movies S3 and S4. (**E**) Wave packet integrated signal [derivation in (*29*)], which helps identify the transition from a formation stage, in which the pump overcomes the dispersion and intrinsic PhP ohmic losses, to the eventual decay. (The effective time scales are indicated in picoseconds.) (**F**) There is a clear correlation between the dispersion rate and the wave packet's group velocity, as expected by theory: Wave packets with higher group velocities are less dispersive. Throughout the figure, the error bars represent a 99% certainty of the fitting process.

lower than the speed of light in vacuum. In a thicker sample, the fastest recorded group velocity is 6.7 μm/ps, which is 45 times lower than the speed of light in vacuum but still sufficiently low for our free-electron probing technique to record the dynamics. An additional measurement includes the propagation over a duration of more than 2.5 ps in a 7.5-nm-thick sample and propagation lengths over distances of more than 12 μm for a 55-nm-thick sample, crossing the entire length of the sample. These propagation distances and durations are a merit of the isotopically pure hBN (^{11}B), which encounters smaller losses than normal hBN flakes (*6*).

The data show a first demonstration of a change in the group velocities of PhP wave packets during their propagation, for which we use the terminology wave packet acceleration and deceleration. We observed this effect in all sample thicknesses (Fig. 3, A to C). For example, in the 7.5-nm sample, the group velocity decreased by a factor of 5 (Fig. 3A). This effect is surprising because the PhP dispersion is expected to cause the slower modes to decay faster, which would result in acceleration rather than deceleration.

We find that this effect reveals a more general S-shaped trajectory for the PhP wave packets: During the pulse excitation (shaded backgrounds in Fig. 3, A to C and E), the wave packet first remains near the edge of the sample (extraordinarily slow group velocity), then experiences fast propagation, and finally decelerates to reach its final steady propagation velocity. The first two regimes are related to the excitation pulse duration and chirp, which pumps the PhP with different spectral components at different times. The measured phenomena of wave packet deceleration and acceleration are consistent with the continuous-PINEM analysis of a set of finite-difference time-domain (FDTD) simulations, as shown in Fig. 3D, fig. S5, and movies S3 and S4. The simulations show that when the pulse is longer, and/or when the chirp is stronger, the change in velocity becomes more dominant, in agreement with our measurements.

Analysis of wave packet dynamics

Our experiment identifies intriguing features of the PhP wave packets during the wave packet formation and free propagation. We integrate over the entire observable signal at each time delay to analyze the competition between the laser pumping to the dispersion and decay. We identify two features in the PhP wave packet

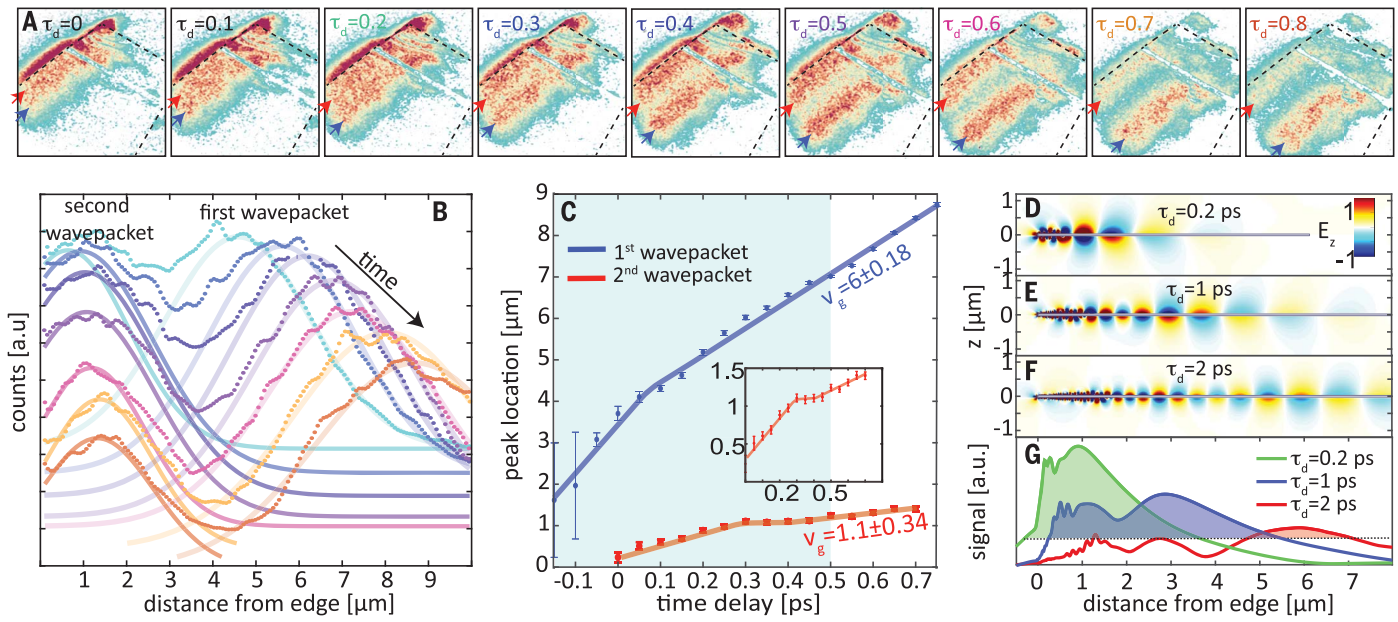

Fig. 4. Observation of a multibranch PhP wave packet that splits into two distinct wave packets of different branches and different group velocities. (**A**) Snapshots at different times of the two wave packets propagating through the sample, with small blue and red arrows marking the peaks of each wave packet. The dashed lines indicate the sample borders. (**B**) Measured signal when averaged along the edge (dotted curves) with the double-Gaussian fit for each measurement (solid curves). The data show two distinct wave packets with different group velocities. The time steps between the curves are 0.1 ps, starting at τ_d = 0.2 ps. (**C**) Locations of the two wave packets as a function of time, extracting the group velocities in units of μm/ps. The shaded background represents times at which the wave packet is still being pumped. The inset shows a zoom-in on the second wave packet trajectory. (**D** to **F**) Simulated *z*-component of the electric field of a 55-nm hBN flake on a 20-nm-thick Si_3N_4 membrane at specific times τ_d, showing an example of wave packet evolution as it splits into multiple individual wave packets of different orders. (**G**) The electron energy–filtered signal, calculated using the fields from (D) to (F) and thus extracting the wave packet profiles above a certain cutoff (shaded area). The signal shows a clear distinction between the wave packet of the first and second modes, similar to the experimental results.

dynamics: The first is the gradual buildup of the wave packet when the pump overcomes the PhP wave packet dispersion and intrinsic ohmic losses (shown as the blue-shaded background in Fig. 3E). We identify cases for which the integrated signal continues to grow even when the wave packet peak is already 10 μm from the edge and is propagating at a stable group velocity (green curves in Fig. 3, C and E). The second feature is that the measured wave packets disperse and decay at different rates (Fig. 3, E and F), quantified by a dispersion time τ (Fig. 3E). The dispersion causes wave packet broadening that reduces the field amplitude and thus also reduces the detected electron signal. The detected electron signal also varies with frequency, because different PhP modes have different confinements [see (*29*) for a quantitative analysis of the signal dependence on PhP confinement]. As a result, the decay in the integrated signal is caused mostly by the wave packet dispersion (subpicosecond time scale) and not by intrinsic ohmic loss (few-picosecond time scale). As expected from theory, shorter dispersion times (i.e., larger dispersion) occur for slower group velocities.

The efficient PINEM interaction enables the measurement of the propagation of multibranch wave packets that split over time into distinguishable Gaussian-like wave packets of different group velocities (Fig. 4 and movie S2). The multibranch wave packets are created because the excitation at each wavelength can couple into more than a single branch in the dispersion relations (Fig. 1B), a phenomenon which was also observed in plasmonic structures (*34*). Figure 4A shows the propagation of a multibranch PhP wave packet that splits into two single-branch wave packets, propagating as a double Gaussian (Fig. 4B). From the location of the double Gaussian peaks (shown in Fig. 4C), we extract two different group velocities for the first- and second-branch wave packets (6 and 1.1 μm/ps, respectively). We enhanced the observation of this effect by changing the electron energy slit to reduce the threshold electric field. As confirmed by the FDTD simulations (Fig. 4, D to G), at short times, the two wave packets completely overlap. Then, at longer times, the wave packets gradually split from one another. Interestingly, as also confirmed by the FDTD simulation, the PINEM-type measurement shows a clear spatial separation between the wave packets while their fields still appear to overlap. It is the electron's sensitivity to the field inside the hBN that enables one to distinguish the individual profiles of the two partially overlapping wave packets.

We found that the PINEM interaction remains efficient for polariton wave packets at higher-order branches. This feature is seen in the experimental data: The first- and second-order PhP branches provide a signal of a similar magnitude (Fig. 4B). Our numerical simulations confirmed this result: Despite the second branch having an overall smaller energy (owing to less efficient coupling), the PINEM signal is of comparable strength. This result arises from the nature of the interaction, whereby the electron integrates along its trajectory and thus includes the field inside the hBN, which is larger because the field is more confined. Higher-branch modes have larger confinement and thus higher field amplitudes, and yet they decay faster along the *z* direction; thus, the integrated signal remains comparable. Most near-field imaging techniques probe the surface of the material and are thus essentially less efficient when the goal is to image wave packets in higher-order branches, because they decay more rapidly along the *z* direction. (The inefficient light out-coupling of the higher branches reduces the signal further.) By using the penetration of free electrons, PINEM-type techniques such

as ours bypass these limits, becoming especially advantageous for imaging higher-branch polaritonic modes and highly confined polaritons in general.

Concluding remarks and outlook

The measured phenomena are fully captured by the linear optical response of hyperbolic media, as verified by our simulations. Finding the nonlinear optical response of hBN is still a topic of ongoing investigation (*43*, *44*) and should require stronger fields compared with the values in our experiments [electric field of ~1.5 MV/m (*29*)]. Future investigation of optical nonlinearities in 2D materials holds potential for the observation of spatiotemporal soliton wave packets of 2D polaritons and previously unobserved forms of 2D shockwaves and light bullets.

Our work builds on key advances in the areas of PINEM, ultrafast electron microscopy, and ultrafast electron diffraction (*25*). Whereas PINEM techniques have examined the temporal dynamics of optical excitations by interference patterns of plasmon polaritons (*26*) and decay of photonic cavity modes (*27*, *28*), our experiments resolve the dynamics of the entire optical wave packet due to the slower group velocities and shorter wave packet extents of PhPs. The slow group velocity causes the wave packet envelope to remain almost static within the duration of the electron interaction (the wave packet moves only a fraction of a micron during the electron's duration; 0.13-ps standard deviation); thus, we can record the wave packet dynamics. In this manner, our experiment is operated at frequencies that are in between the optical range and the range of mechanical vibrations (typically at gigahertz frequencies), where the dynamics of phonons was observed because of their slow oscillation relative to the duration of the electron probe (*22*, *24*). The PhPs in our experiment differ from these mechanical vibrations by being coherent optical excitations, which are in fact hybrids of the mechanical vibrations (optical phonons) and photons in the IR region. Consequently, the imaging of polaritons in 2D materials uses advantages from both plasmon imaging (*26*) and phonon imaging (*22*, *24*).

REFERENCES AND NOTES

1. M. Jablan, H. Buljan, M. Soljacic, *Phys. Rev. B* **80**, 245435 (2009).
2. D. N. Basov, A. Asenjo-Garcia, P. J. Schuck, X. Zhu, A. Rubio, *Nanophotonics* **10**, 549–577 (2020).
3. V. W. Brar, M. C. Sherrott, D. Jariwala, *Chem. Soc. Rev.* **47**, 6824–6844 (2018).
4. P. Li *et al*., *Nat. Commun.* **6**, 7507 (2015).
5. K. Chaudhary *et al*., *Sci. Adv.* **5**, eaau7171 (2019).
6. A. J. Giles *et al*., *Nat. Mater.* **17**, 134–139 (2018).
7. D. Alcaraz Iranzo *et al*., *Science* **360**, 291–295 (2018).
8. W. Ma *et al*., *Nature* **562**, 557–562 (2018).
9. Y. Kurman, I. Kaminer, *Nat. Phys.* **16**, 868–874 (2020).
10. N. Rivera, I. Kaminer, *Nat. Rev. Phys.* **2**, 538–561 (2020).
11. I. Epstein *et al*., *Science* **368**, 1219–1223 (2020).
12. A. M. Weiner, *Rev. Sci. Instrum.* **71**, 1929–1960 (2000).
13. P. Colman *et al*., *Nat. Photonics* **4**, 862–868 (2010).
14. M. A. Noginov *et al*., *Appl. Phys. Lett.* **94**, 151105 (2009).
15. A. Poddubny, I. Iorsh, P. Belov, Y. Kivshar, *Nat. Photonics* **7**, 948–967 (2013).
16. K. V. Sreekanth, A. De Luca, G. Strangi, *Appl. Phys. Lett.* **103**, 023107 (2013).
17. S. Dai *et al*., *Science* **343**, 1125–1129 (2014).
18. E. Yoxall *et al*., *Nat. Photonics* **9**, 674–678 (2015).
19. B. Barwick, D. J. Flannigan, A. H. Zewail, *Nature* **462**, 902–906 (2009).
20. F. J. García de Abajo, A. Asenjo-Garcia, M. Kociak, *Nano Lett.* **10**, 1859–1863 (2010).
21. S. T. Park, M. Lin, A. H. Zewail, *New J. Phys.* **12**, 123028 (2010).
22. D. T. Valley, V. E. Ferry, D. J. Flannigan, *Nano Lett.* **16**, 7302–7308 (2016).
23. T. T. A. Lummen *et al*., *Nat. Commun.* **7**, 13156 (2016).
24. D. R. Cremons, D. A. Plemmons, D. J. Flannigan, *Nat. Commun.* **7**, 11230 (2016).
25. Y. Morimoto, P. Baum, *Nat. Phys.* **14**, 252–256 (2018).
26. I. Madan *et al*., *Sci. Adv.* **5**, eaav8358 (2019).
27. K. Wang *et al*., *Nature* **582**, 50–54 (2020).
28. O. Kfir *et al*., *Nature* **582**, 46–49 (2020).
29. See supplementary materials.
30. R. Hillenbrand, T. Taubner, F. Keilmann, *Nature* **418**, 159–162 (2002).
31. M. A. Huber *et al*., *Nat. Nanotechnol.* **12**, 207–211 (2017).
32. M. Mrejen, L. Yadgarov, A. Levanon, H. Suchowski, *Sci. Adv.* **5**, eaat9618 (2019).
33. A. J. Sternbach *et al*., *Science* **371**, 617–620 (2021).
34. B. Frank *et al*., *Sci. Adv.* **3**, e1700721 (2017).
35. A. Polman, M. Kociak, F. J. García de Abajo, *Nat. Mater.* **18**, 1158–1171 (2019).
36. R. F. Egerton, *Electron Energy-Loss Spectroscopy in the Electron Microscope* (Springer, 2011).
37. O. L. Krivanek *et al*., *Nature* **514**, 209–212 (2014).
38. X. Li *et al*., *Science* **371**, 1364–1367 (2021).
39. F. S. Hage *et al*., *Sci. Adv.* **4**, eaar7495 (2018).
40. N. Li *et al*., *Nat. Mater.* **20**, 43–48 (2021).
41. J. Nelayah *et al*., *Nat. Phys.* **3**, 348–353 (2007).
42. O. Reinhardt, I. Kaminer, *ACS Photonics* **7**, 2859–2870 (2020).
43. M. Mehdi Jadidi *et al*., paper FTh4A.6 presented at the 2020 Conference on Lasers and Electro-Optics (CLEO), San Jose, CA, 10 to 15 May 2020.
44. A. A. Popkova *et al*., *ACS Photonics* **8**, 824–831 (2021).

ACKNOWLEDGMENTS

We thank G. Eisenstein, M. Segev, and G. Bartal for the fruitful discussions regarding this manuscript. We thank IDES Ltd. and especially S. T. Park for support, advice, and discussions. The experiments were performed on the UTEM of the AdQuanta group of I.K., which is installed inside the electron microscopy center (MIKA) of the Department of Materials Science and Engineering at the Technion. **Funding:** This project has received funding from the European Union's Horizon 2020 research and innovation program under grant agreement no. 851780-ERC-NanoEP, the Israel Science Foundation (grant no. 830/19), and the Binational USA-Israel Science Foundation (BSF) 2018288. Y.K. is supported by a Gutwirth and Jacobs Fellowship. hBN crystal growth was supported by National Science Foundation grant CMMI 1538127. F.H.L.K. acknowledges support from the government of Spain (FIS2016-81044; Severo Ochoa CEX2019-000910-S), Fundació Cellex, Fundació Mir-Puig, and Generalitat de Catalunya (CERCA, AGAUR, SGR 1656). Furthermore, the research leading to these results has received funding from the European Union's Horizon 2020 under grant agreement no. 881603 (Graphene flagship Core3) and the ERC TOPONANOP under grant agreement n° 726001. **Author contributions:** Y.K. and I.K. conceived the project and designed the experiments. R.D. constructed the experimental setup. Y.K., R.D., K.W., M.Y., and Y.A. conducted the experimental measurements. O.R. developed the theory. Y.K. performed the numerical simulations. Y.K., H.H.S., F.H.L.K., M.K., and I.K. wrote the manuscript. L.H.G.T., S.Y.W., and M.K. fabricated the first hBN samples and helped in initiating this research. J.L. and J.H.E. fabricated the isotopically pure hBN, and H.H.S. performed its exfoliation into a TEM membrane. All authors reviewed and discussed the manuscript and made substantial contributions to it. **Competing interests:** None declared. **Data and materials availability:** All data needed to evaluate the conclusions in the paper are present in the paper or the supplementary materials.

SUPPLEMENTARY MATERIALS

science.sciencemag.org/content/372/6547/1181/suppl/DC1
Materials and Methods
Supplementary Text
Figs. S1 to S7
Table S1
References (*45*–*61*)
Movies S1 to S4

3 February 2021; accepted 4 May 2021
10.1126/science.abg9015

Science

Spatiotemporal imaging of 2D polariton wave packet dynamics using free electrons

Yaniv Kurman, Raphael Dahan, Hanan Herzig Sheinfux, Kangpeng Wang, Michael Yannai, Yuval Adiv, Ori Reinhardt, Luiz H. G. Tizei, Steffi Y. Woo, Jiahan Li, James H. Edgar, Mathieu Kociak, Frank H. L. Koppens and Ido Kaminer

Science **372** (6547), 1181-1186.
DOI: 10.1126/science.abg9015

Imaging polariton dynamics

Two-dimensional (2D) materials can confine light to volumes much shorter than the wavelength, and, together, the long propagation lengths make them attractive materials for developing nanophotonic platforms. Characterizing the spatiotemporal control of 2D polariton wave packets has been hindered for the same reasons that make their potential applications exciting: They have extremely small wavelengths and are strongly confined inside the material. Kurman *et al.* developed a new pump-probe technique based on electron emission that provides access to the spatiotemporal dynamics of 2D polaritons. The nanometric spatial resolution and femtosecond temporal resolution will be useful for probing the excitation dynamics of these materials.

Science, abg9015, this issue p. 1181

Science (print ISSN 0036-8075; online ISSN 1095-9203) is published by the American Association for the Advancement of Science, 1200 New York Avenue NW, Washington, DC 20005. The title *Science* is a registered trademark of AAAS.